

# Resonant production of spin-3/2 color octet electron at the LHeC

M. Şahin\*

*Uşak University, Department of Physics, Uşak, Turkey.*

## Abstract

In this work, we investigate resonant production of spin-3/2 color octet electron at the Large Hadron electron Collider (LHeC). Signal and background analysis are performed and discovery, observation and exclusion limits are determined for spin 3/2 color octet electron masses. Reachable values of the compositeness scale are presented as a function of the spin-3/2 color octet electron masses.

---

\* mehmet.sahin@usak.edu.tr

## I. INTRODUCTION

Standard Model (SM) of particle physics successfully explains electromagnetic, weak and strong interactions of fundamental particles. SM predictions are consistent with numerous experiments. Furthermore, results of the ATLAS and the CMS Collaborations [1, 2] are consistent with the SM Higgs boson hypothesis. If the new particle is the SM Higgs boson, why the fundamental particles have mass is explained by SM. However, SM does not explain some cases such as quark-lepton symmetry, family replication, hierarchy problems, charge quantization, etc. Many theoretical hypothesis are proposed to clarify these cases. Supersymmetry (SUSY), extra dimensions, grand unified theories (GUTs) and compositeness seem to be most promising candidates for beyond the SM physics.

The subjects of family replication and quark-lepton symmetry are explained in the best manner by compositeness. In the framework of composite models quarks, leptons and gauge bosons are composite particles made up of more basic constituents. These basic constituents are named preons. The preonic models lead to a rich spectrum of new type particles such as diquarks, leptoquarks, leptogluons, dileptons and excited fermions etc.

We have interested in color octet leptons which are predicted in all composite models with colored preons [3–9]. For example, in the framework of fermion-scalar models, leptons would be a bound state of one fermionic preon and one scalar antipreon  $l = (F\bar{S}) = 1 \oplus 8$  (both F and S are color triplets), then each SM lepton is thought to accompany with its own color octet partner [9]. Color octet electrons have the same status as the excited leptons. As the excited leptons, color octet electrons have a spin of  $1/2$  or  $3/2$ . The motivation for spin- $3/2$  leptons comes from composite models [10, 11] and supergravity gauge theories [12]. Spin- $1/2$  color octet electron are investigated in earlier papers [9, 13–17]. Recently spin- $1/2$  color octet electron have been analyzed for future high energy colliders: Large Hadron electron Collider (LHeC) [18], International Linear Collider (ILC) and Compact Linear Collider (CLIC) [19] and Large Hadron Collider (LHC) [20]. Although spin- $3/2$  color octet electrons are mentioned in literature, they have not been investigated in details up to now. In order to close this gap in the literature, we investigate resonant production of the spin- $3/2$  color octet electron at the LHeC.

LHeC project supported by CERN, ECFA and NuPECC is a new LHC based electron-proton and electron-ion collider [21]. LHeC is under design for synchronous operation with

| Stage                           | $E_e$ , GeV | $\sqrt{s}$ , TeV | $L$ , $10^{33} \text{ cm}^{-2} \text{ s}^{-1}$ |
|---------------------------------|-------------|------------------|--|
| Lower-energy LHeC ERL (LHeC-1)  | 60          | 1.296            | 1  |
| Higher-energy LHeC ERL (LHeC-2) | 150         | 2.049            | 100  |

Table I. Tentative parameters of the LHeC linac-ring options. ERL denotes energy recovery linac.

the LHC at CERN in the twenties. Conceptual design report (CDR) of the LHeC is completed and published last summer [22]. The CDR of the LHeC describes two options for the LHeC, a ring-ring (RR) and a linac-ring (LR) configuration. After the CDR was completed, it was decided to continue the technical design work for the linac-ring (LR) configuration in a recent workshop [23, 24]. History and status of linac-ring type collider proposals can be found in review [25]. We have preferred two energy options of linac-ring (LR) type LHeC in our calculations. The first one is lower-energy LHeC ERL option (see LHeC CDR [22] section 7.1.2). The lepton beam energy is 60 GeV and proton beam energy is 7000 GeV in this option. Electron-proton luminosity is  $10^{33} \text{ cm}^{-2} \text{ s}^{-1}$ . The latter option is higher-energy LHeC ERL option (see LHeC CDR [22] section 7.1.5). The lepton beam energy is 150 GeV and proton beam energy is 7000 GeV in this option. Electron-proton luminosity is  $10^{35} \text{ cm}^{-2} \text{ s}^{-1}$ . These properties of LHeC are shown in Table 1.

In this paper, we consider resonant production of spin-3/2 color octet electron ( $e_8$ ) at the Large Hadron electron Collider. In the Section II, the interaction Lagrangian of spin-3/2 leptogluons, decay widths and resonant production cross sections of spin-3/2 color octet electron at different stages of the LHeC are presented. In Section III, signal and background analysis are performed at the LHeC and achievable masses and compositeness scale are determined for spin-3/2 color octet electrons. Finally, we give concluding remarks in Section IV.

## II. INTERACTION LAGRANGIAN, DECAY WIDTH AND CROSS SECTIONS

For the interaction of spin-3/2 leptogluons with corresponding lepton and gluon we use following Lagrangian:

$$L = \frac{1}{\Lambda^2} \sum_l \{ \bar{l}_8^\alpha g_s \partial^\mu G_{\mu\nu}^\alpha \sigma^{\mu\nu} (\eta_L l_L + \eta_R l_R) + h.c. \}, \quad (1)$$

where  $\bar{l}_8^\alpha$  is a Rarita-Schwinger vector spinor [26] field for spin-3/2 leptogluons, index  $\alpha = 1, 2, \dots, 8$  denotes color,  $g_s$  is gauge coupling,  $G_{\mu\nu}^\alpha$  is the field strength tensor for gluon,  $\sigma^{\mu\nu}$  is the anti-symmetric tensor,  $\eta_L$  and  $\eta_R$  are the chirality factors,  $l_L$  and  $l_R$  represent left and right spinor components of leptons and  $\Lambda$  is the compositeness scale. We introduce only the first family leptogluons in this articles. We assume that the leptogluon of the first family will be lighter than the others following what we observe experimentally in SM. The leptonic chirality conservation requires  $\eta_L \eta_R = 0$  and following the almost exclusively left-handed neutrinos, that we observe in the nature, we set  $\eta_L = 1$  and  $\eta_R = 0$  in our calculations. Propagator of spin-3/2 color octet electron is represented by equation 2.

$$P^{\mu\nu} = \frac{1}{p^2 - M_{e_8}^2} [-(\gamma^\mu p_\mu + M_{e_8})(g^{\mu\nu} - \frac{p^\mu p^\nu}{M_{e_8}^2}) - \frac{1}{3}(\gamma^\mu + \frac{p^\mu}{M_{e_8}})(\gamma^\nu p_\nu - M_{e_8})(\gamma^\nu + \frac{p^\nu}{M_{e_8}})] \quad (2)$$

Decay width of spin-3/2 color octet electrons is given by

$$\Gamma_{e_8} = \frac{\alpha_s M_{e_8}^5}{12\Lambda^4}. \quad (3)$$

The analytic expression for partonic level differential cross-section for the process  $e^- p \rightarrow e_8 \rightarrow ge^-$  is given by

$$\frac{d\hat{\sigma}}{d\hat{t}}(e^- p \rightarrow e_8 \rightarrow ge^-) = -\frac{64\alpha_s^2 \hat{s} \hat{t} (\frac{\hat{s}^2}{M_{e_8}^2} - 3(\hat{s} + \hat{t}))^2 \pi}{\alpha_s^2 M_{e_8}^{12} + 144\Lambda^8 (M_{e_8}^2 - \hat{s})^2}. \quad (4)$$

where  $\hat{s}$  and  $\hat{t}$  are Mandelsam variables,  $\alpha_s$  is strong coupling constant and  $\hat{\sigma}$  is partonic cross-section.

For the numerical calculations we implement this Lagrangian into the CALCHEP program [27, 28]. Figure 1 presents decay widths of spin-3/2 color octet electrons for  $\Lambda = M_{e_8}$ ,  $\Lambda = 5$  TeV and  $\Lambda = 10$  TeV.

Resonant production cross sections of spin-3/2 color octet electrons for the two stages of the LHeC which are in Table 1, are calculated using CALCHEP with CTEQ6L [29] parton distribution functions. In these calculations, we used factorization scale  $Q^2 = M_{e_8}^2$ . Figure 2 presents resonant production cross sections of spin-3/2 color octet electrons for  $\Lambda = M_{e_8}$ ,  $\Lambda = 5$  TeV and  $\Lambda = 10$  TeV at the LHeC-1 with  $\sqrt{s} = 1.296$  TeV. It is seen from Figure 2 that spin-3/2 color octet electrons have sufficiently high cross-section values for  $\Lambda = M_{e_8}$  and  $\Lambda = 5$  TeV even at the high mass values of  $e_8$ . Figure 3 shows resonant production cross

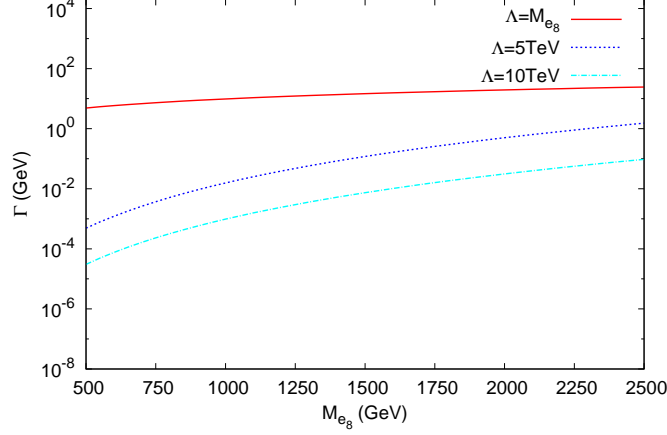


Figure 1. Spin-3/2 color octet electron decay width via its mass for  $\Lambda = M_{e_8}$ ,  $\Lambda = 5$  TeV and  $\Lambda = 10$  TeV.

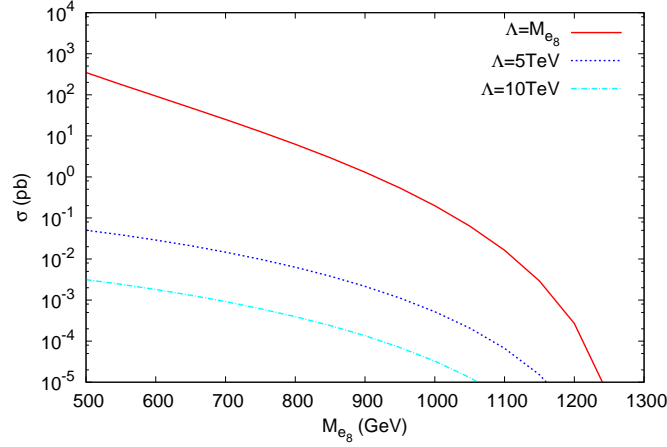


Figure 2. Resonant production of spin-3/2 color octet electrons at the LHeC-1 with  $\sqrt{s} = 1.296$  TeV.

section of spin-3/2 color octet electrons for  $\Lambda = M_{e_8}$ ,  $\Lambda = 5$  TeV and  $\Lambda = 10$  TeV at the LHeC-2 with  $\sqrt{s} = 2.049$  TeV. It is seen from Figure 3 that spin-3/2 color octet electrons have sufficiently high cross-section for  $\Lambda = M_{e_8}$ ,  $\Lambda = 5$  TeV, and  $\Lambda = 10$  TeV at the high mass values of  $e_8$ .

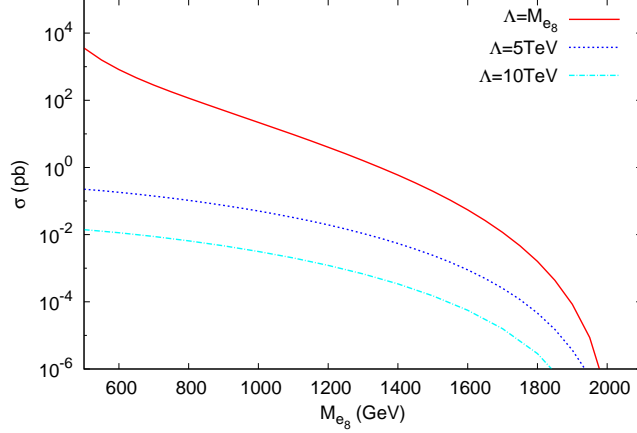


Figure 3. Resonant production of spin-3/2 color octet electrons at the LHeC-2 with  $\sqrt{s} = 2.049$  TeV.

### III. SIGNAL AND BACKGROUND ANALYSIS

#### A. Lower-energy LHeC ERL stage (LHeC-1 with $\sqrt{s} = 1.296$ TeV and $L_{int} = 10 fb^{-1}$ )

The center of mass energy of this LHeC option is 1.296 TeV and integrated luminosity is  $L_{int} = 10 fb^{-1}$ . Our signal process is  $ep \rightarrow e_8 \rightarrow eg + X$  and background process is  $ep \rightarrow ej + X$  through  $\gamma$  and  $Z$  exchange, where  $g$  denotes gluon and  $j$  represents jets which are composed of quarks ( $u, \bar{u}, d, \bar{d}, c, \bar{c}, s, \bar{s}, b, \bar{b}$ ) for background. In order to determine appropriate cuts we need transverse momentum ( $P_T$ ) and pseudo-rapidity ( $\eta$ ) distributions of signal and background processes.

Figure 4 presents normalized transverse momentum distributions of final state jets for signal with  $\Lambda = 5$  TeV for left panel and signal with  $\Lambda = M_{e_8}$  for right panel and also background for both panels. The final state electron's normalized transverse momentum distributions are the same as the plots of the final state jets in Figure 4. It is seen from Figure 4 that  $P_T > 50$  GeV cut for both final states essentially reduces background but signal is almost unchanged. Left and right panels in Figure 5 represent normalized pseudo-rapidity ( $\eta$ ) distributions of electrons for signal with  $\Lambda = 5$  TeV and signal with  $\Lambda = M_{e_8}$  and also for background, respectively. It is seen from left and right panels of Figure 5,  $\eta_{e^-}$  distributions of signal drastically different from  $\eta_{e^-}$  distributions of background. In addition, most of background lie in  $0 < \eta_{e^-} < 2$  region for both panels in Figure 5. Left and right

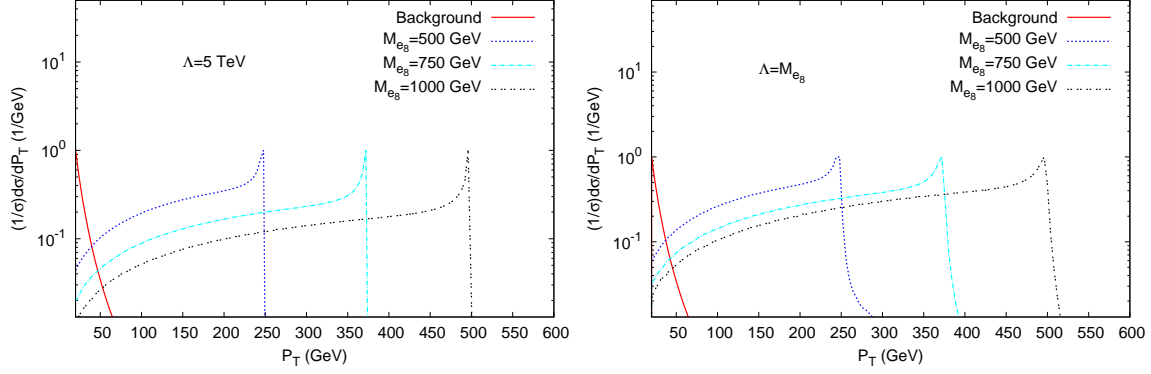


Figure 4. Left: Normalized transverse momentum ( $P_T$ ) distributions of signal with  $\Lambda = 5$  TeV and background at the LHeC-1 with  $\sqrt{s} = 1.296$  TeV. Right: Normalized transverse momentum ( $P_T$ ) distributions of signal with  $\Lambda = M_{e_8}$  TeV and background at the LHeC-1 with  $\sqrt{s} = 1.296$  TeV.

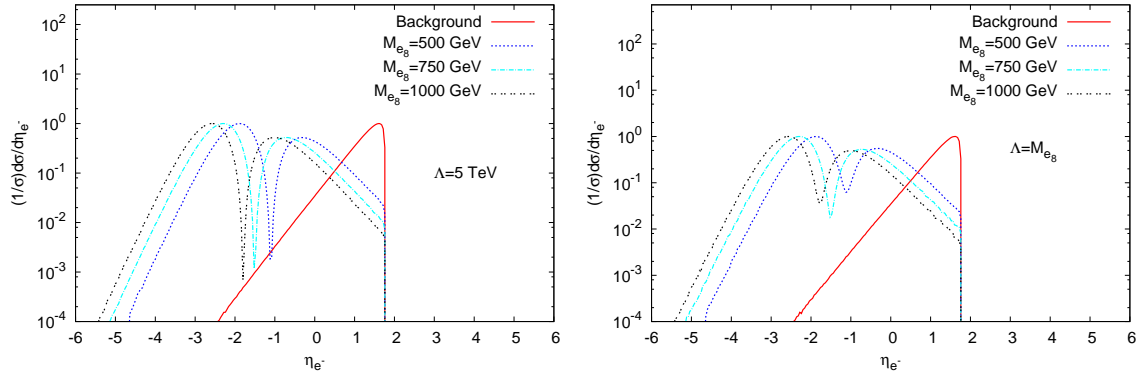


Figure 5. Left: Normalized pseudo-rapidity distributions of final state electrons for signal with  $\Lambda = 5$  TeV and background at the LHeC-1 with  $\sqrt{s} = 1.296$  TeV. Right: Normalized pseudo-rapidity distributions of final state electrons for signal with  $\Lambda = M_{e_8}$  and background at the LHeC-1 with  $\sqrt{s} = 1.296$  TeV.

panels in Figure 6 present normalized pseudo-rapidity ( $\eta$ ) distributions of jets for signal with  $\Lambda = 5$  TeV for left panel and signal with  $\Lambda = M_{e_8}$  for right panel and also for background (both panels), respectively. In Figure 6,  $\eta_j$  distributions for signal and background are not drastically different. For this reason, we select pseudo-rapidity cuts values as follows:  $-4 < \eta_e < -0.8$  for final state electron and  $-4 < \eta_j < 1.5$  for final state jets. We present the invariant mass distributions for signal with  $\Lambda = 5$  TeV for left panel and signal  $\Lambda = M_{e_8}$  right panel and also for background (both panels) in Figure 7.

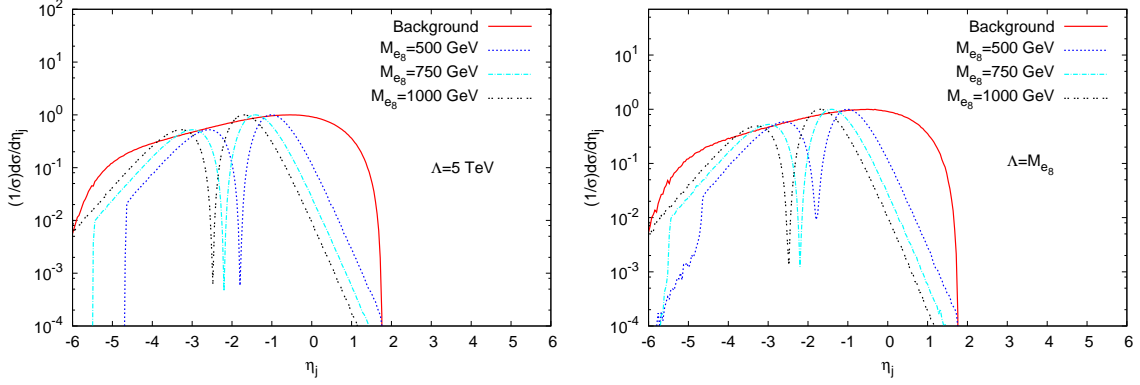


Figure 6. Left: Normalized pseudo-rapidity distributions of final state jets for signal with  $\Lambda = 5$  TeV and background at the LHeC-1 with  $\sqrt{s} = 1.296$  TeV. Right: Normalized pseudo-rapidity distributions of final state jets for signal with  $\Lambda = M_{e_8}$  TeV and background at the LHeC-1 with  $\sqrt{s} = 1.296$  TeV.

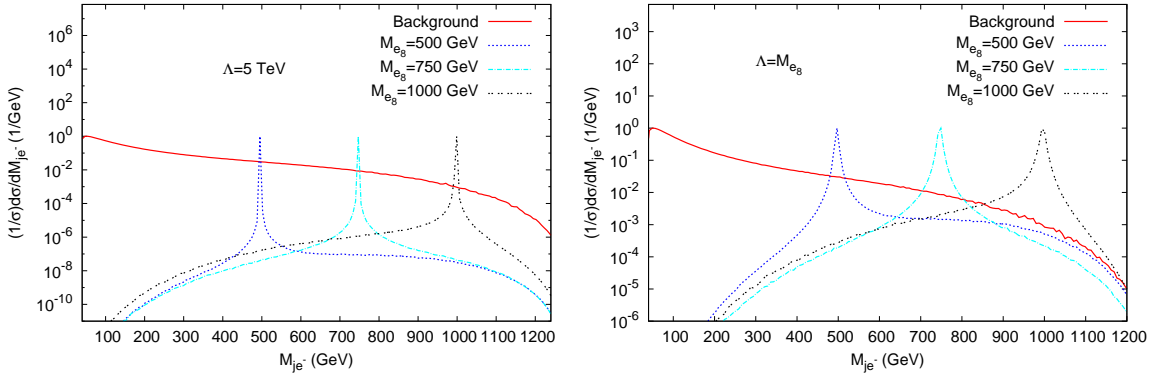


Figure 7. Left: Normalized invariant mass distributions for signal with  $\Lambda = 5$  TeV and background at the LHeC-1 with  $\sqrt{s} = 1.296$  TeV. Right: Normalized invariant mass distributions for signal with  $\Lambda = M_{e_8}$  and background at the LHeC-1 with  $\sqrt{s} = 1.296$  TeV.

In order to extract the spin-3/2 color octet electron ( $e_8$ ) signals (for the  $\Lambda = 5$  TeV and  $\Lambda = M_{e_8}$ ) and to suppress the backgrounds we used  $P_T > 50$  GeV for all final state electron and jets (these cut values are determined by Figure 4),  $-4 < \eta_{e^-} < -0.8$  for final state electron and  $-4 < \eta_j < 1.5$  for final state jets (these cut values are determined by Figure 5 and Figure 6). In addition to these cut values, we used mass windows as  $M_{e_8} - 10$  GeV  $< M_{je^-} < M_{e_8} + 10$  GeV for signal with  $\Lambda = 5$  TeV and for background. It is seen from Figure 1, signal decay width values are quite small when they are compared to 10 GeV for



| $M_{e_8}$ , GeV | $\Lambda = 5$ TeV |       | $\Lambda = M_{e_8}$ |       |
|-----------------|-------------------|-------|---------------------|-------|
|                 | $N_s$             | $N_b$ | $N_s$               | $N_b$ |
| 500             | 304               | 1268  | 3559200             | 2538  |
| 600             | 185               | 838   | 1053100             | 1678  |
| 700             | 100               | 514   | 308510              | 1028  |
| 800             | 45                | 279   | 82767               | 558   |
| 900             | 16                | 126   | 18617               | 252   |
| 1000            | 4                 | 43    | 3066                | 86    |
| 1100            | —                 | 9     | 278                 | 18    |
| 1200            | —                 | —     | 6                   | 1     |

Table II. The number of signal and background events for the LHeC-1 with  $L_{int} = 10 fb^{-1}$ . Here,  $N_s$  is number of signal events and  $N_b$  is number of background events.

the  $\Lambda = 5$  TeV. We also used mass window as  $M_{e_8} - 20$  GeV  $< M_{je^-} < M_{e_8} + 20$  GeV for signal with  $\Lambda = M_{e_8}$  and for background. As it seen from Figure 1, signal decay width values approximately are 10 GeV at the LHeC-1 kinematic limit (1296 GeV) for the  $\Lambda = M_{e_8}$ .

By using cut sets that are mentioned above and  $L_{int} = 10 fb^{-1}$  integrated luminosity values of the LHeC-1, we have calculated event numbers for some mass values of  $e_8$  and background. We present these event numbers in Table 2.

For statistical significance, we use the following formula [30]

$$S = \sqrt{2[(N_s + N_b) \ln(1 + \frac{N_s}{N_b}) - N_s]}, \quad (5)$$

where  $N_s$  and  $N_b$  represents the number of signal and background events, respectively. The statistical significances of spin-3/2 color octet electron signal with  $\Lambda = 5$  TeV are shown in Figure 8 for the LHeC-1 with  $\sqrt{s} = 1.296$  TeV and  $L_{int} = 10 fb^{-1}$ .

It is seen from Figure 8, upper mass limit for discovery ( $5\sigma$ ) of spin-3/2 color octet electron ( $e_8$ ) is 660 GeV at the LHeC-1 with  $\sqrt{s} = 1.296$  TeV. The upper observation ( $3\sigma$ ) mass limits of  $e_8$  is 777 GeV and the upper exclusion ( $2\sigma$ ) mass limits of  $e_8$  is 849 GeV at the LHeC-1 with  $\sqrt{s} = 1.296$  TeV these values are obtained for  $L_{int} = 10 fb^{-1}$  and  $\Lambda = 5$  TeV. For the  $\Lambda = M_{e_8}$  and  $L_{int} = 10 fb^{-1}$ , the statistical significances of spin-3/2 color octet electron signal at the LHeC-1 with  $\sqrt{s} = 1.296$  TeV are shown in Figure 9. It is seen from

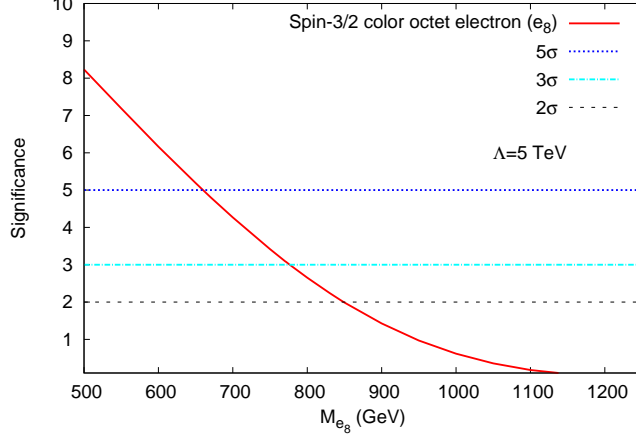


Figure 8. The signal significances as a function of spin-3/2 color octet electron mass at the LHeC-1 with  $\sqrt{s} = 1.296$  TeV. This figure is obtained for  $L_{int} = 10 fb^{-1}$  and  $\Lambda = 5$  TeV.

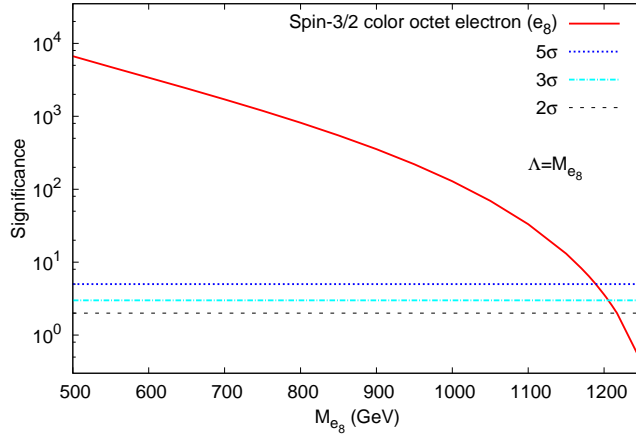


Figure 9. The signal significances as a function of spin-3/2 color octet electron mass at the LHeC-1 with  $\sqrt{s} = 1.296$  TeV. This figure is obtained for  $L_{int} = 10 fb^{-1}$  and  $\Lambda = M_{e_8}$ .

Figure 9, upper mass limit for discovery ( $5\sigma$ ) of spin-3/2 color octet electron ( $e_8$ ) is 1.19 TeV at the LHeC-1 with  $\sqrt{s} = 1.296$  TeV. The upper observation ( $3\sigma$ ) mass limits of  $e_8$  is 1.21 TeV and the upper exclusion ( $2\sigma$ ) mass limits of  $e_8$  is 1.22 TeV at the LHeC-1 with  $\sqrt{s} = 1.296$  TeV. These values are obtained for the compositeness scale  $\Lambda = M_{e_8}$  and the integrated luminosity  $L_{int} = 10 fb^{-1}$ .

Spin-1/2 color octet electron decays into gluon and electron [9, 13, 14, 16–20, 31] like as spin-3/2 color octet electron. Namely they will have same final state in detector. In order to separate spin-3/2 color octet electron signal from spin-1/2 color octet electron signal, we

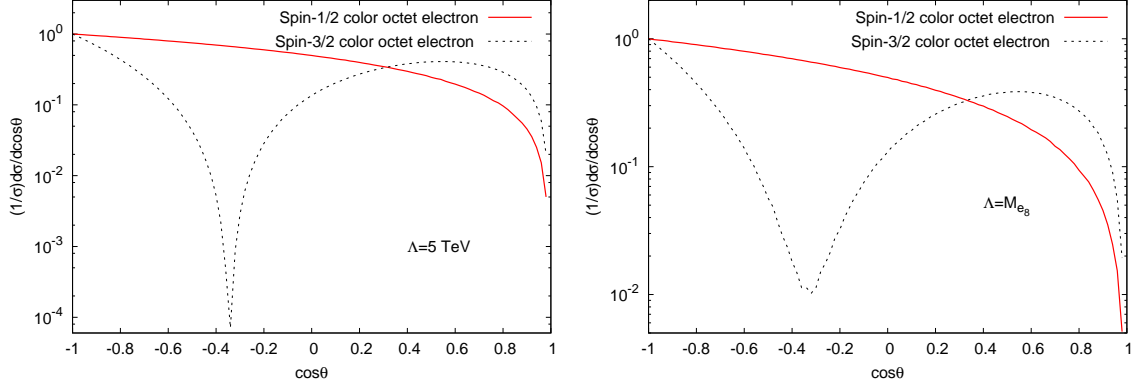


Figure 10. Left: The differential cross section as a function the scattering angle for the spin-3/2 color octet electron ( $\Lambda = 5$  TeV), and the spin-1/2 color octet electron ( $\Lambda = 5$  TeV) at the LHeC-1 with  $\sqrt{s} = 1.296$  TeV. Right: The differential cross section as a function the scattering angle for the spin-3/2 color octet electron ( $\Lambda = M_{e8}$ ), and the spin-1/2 color octet electron ( $\Lambda = M_{e8}$ ) at the LHeC-1 with  $\sqrt{s} = 1.296$  TeV. In the both panels, spin-1/2 and spin-3/2 color octet electron mass values are taken as 500 GeV.

plot normalized differential cross sections as a function of  $\cos\theta$  in Figure 10. The spin-1/2 color octet electron is produced mostly in backward direction and its minimum cross section values are in forward direction. However, spin-3/2 color octet electron is produced mostly in both directions (forward and backward) and its minimum cross section values are between in -0.4 to -0.3. Therefore, the spin-3/2 color octet electron shows more different angular shape than the spin-1/2 color octet electron.

We have calculated the compositeness scale values for some spin-3/2 color octet masses at the LHeC-1 with  $\sqrt{s} = 1.296$  TeV and  $L_{int} = 10 fb^{-1}$ . These values are presented as a function of spin-3/2 color octet electron mass in Fig 11 and in Table 3.

It is seen from table 3 that the spin-3/2 color octet electron with  $M_{e8} = 500$  GeV can be discovered up to 5.68 TeV compositeness scale value at the LHeC-1 ( $\sqrt{s} = 1.296$  TeV and  $L_{int} = 10 fb^{-1}$ ).

## B. Higher-energy LHeC ERL (LHeC-2 with $\sqrt{s} = 2.049$ TeV and $L_{int} = 1000 fb^{-1}$ )

This LHeC option's the center of mass energy is 2.049 TeV and integrated luminosity is  $L_{int} = 1000 fb^{-1}$ . As mentioned in previous subsection, our signal process is  $ep \rightarrow$

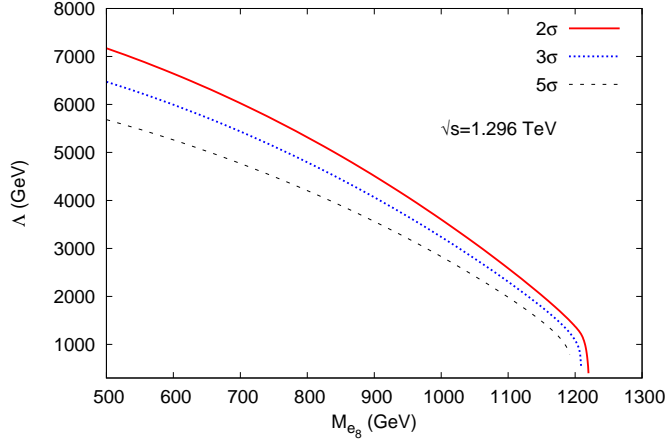


Figure 11. Reachable values of the compositeness scale as a function of spin-3/2 color octet electron mass for the LHeC-1 with  $\sqrt{s} = 1.296$  TeV and  $L_{int} = 10 fb^{-1}$ .

| $M_{e8}, \text{ GeV}$ | $\Lambda, \text{ TeV}$ |           |           |
|-----------------------|------------------------|-----------|-----------|
|                       | $5\sigma$              | $3\sigma$ | $2\sigma$ |
| 500                   | 5.68                   | 6.47      | 7.17      |
| 600                   | 5.28                   | 6.01      | 6.66      |
| 700                   | 4.80                   | 5.47      | 6.07      |
| 800                   | 4.24                   | 4.85      | 5.38      |
| 900                   | 3.61                   | 4.13      | 4.59      |
| 1000                  | 2.89                   | 3.32      | 3.69      |
| 1100                  | 2.05                   | 2.39      | 2.68      |

Table III. Reachable values of the compositeness scale for some spin-3/2 electrons mass values at the LHeC-1 with  $\sqrt{s} = 1.296$  TeV and  $L_{int} = 10 fb^{-1}$ .

$e_8 \rightarrow eg + X$  and background process is  $ep \rightarrow ej + X$  through  $\gamma$  and  $Z$  exchange, where  $g$  represents gluon and  $j$  represents jets that are composed of quarks ( $u, \bar{u}, d, \bar{d}, c, \bar{c}, s, \bar{s}, b, \bar{b}$ ). In order to reduce backgrounds and obtain clear signal, we need to apply some cuts. So, transverse momentum ( $P_T$ ) and pseudo-rapidity ( $\eta$ ) distributions of signal and background processes are used for determining appropriate cuts. Figure 12 presents normalized transverse momentum distributions of final state jets for signal with  $\Lambda = 5$  TeV for left panel, signal with  $\Lambda = M_{e8}$  for right panel and also for background (both panels).

Normalized transverse momentum distributions of final state electron for signal with  $\Lambda = 5$  TeV and signal with  $\Lambda = M_{e_8}$  and also for background are the same as normalized transverse momentum distributions of the final state jets in Figure 12. It is seen from left and right panels of Figure 12,  $P_T > 50$  GeV cuts for the final state electron and jets essentially reduces background but signal is almost unchanged. Left and right panels in Figure 13 represent normalized pseudo-rapidity ( $\eta$ ) distributions of electron for signal with  $\Lambda = 5$  TeV and signal with  $\Lambda = M_{e_8}$  and also for background, respectively. As it seen from left and right panels of Figure 13,  $\eta_{e^-}$ -distributions of signal drastically different from  $\eta_{e^-}$  distributions of background. It is seen that most of background lie in  $0 < \eta_{e^-} < 3$  region in both panels of Figure 13. Left and right panels in Figure 14 present normalized pseudo-rapidity ( $\eta$ ) distributions of jets for signal with  $\Lambda = 5$  TeV for left panel, signal with  $\Lambda = M_{e_8}$  for right panel and also for background (both panels), respectively. As it is seen from Figure 14 in both left and right panels,  $\eta_j$  distributions for signal and background are not drastically different. Transverse momentum ( $P_T$ ) and pseudo-rapidity distributions ( $\eta$ ) of signal with  $\Lambda = 10$  TeV give the same knowledge as transverse and pseudo-rapidity distributions of signal with  $\Lambda = 5$  TeV and  $\Lambda = M_{e_8}$ . Therefore, these distributions of signal with  $\Lambda = 10$  TeV are not given in text. Taking advantage of the this kinematical distributions, we select pseudo-rapidity cuts values as follows:  $-4 < \eta_{e^-} < -0.3$  for final state electron and  $-4 < \eta_j < 2$  for final state jets. We present the invariant mass distributions for signal with  $\Lambda = 5$  TeV for left panel, signal  $\Lambda = M_{e_8}$  for right panel and also for background (both panels) in Figure 15.

In order to extract the spin-3/2 color octet electron ( $e_8$ ) signals for the  $\Lambda = 10$  TeV,  $\Lambda = 5$  TeV and  $\Lambda = M_{e_8}$  and to suppress the backgrounds we used  $P_T > 50$  GeV for all final state electron and jets (these cut values are determined by Figure 12),  $-4 < \eta_{e^-} < -0.3$  for final state electron and  $-4 < \eta_j < 2$  for final state jets (these cut values are determined by Figure 13 and Figure 14). In addition to these cut values, we have used mass window as  $M_{e_8} - 10 \text{ GeV} < M_{je^-} < M_{e_8} + 10 \text{ GeV}$  for signal with  $\Lambda = 10$  TeV,  $\Lambda = 5$  TeV and also for background. In view of the fact that it is seen from Figure 1, signal decay width values are much more smaller than 10 GeV for the  $\Lambda = 10$  TeV and  $\Lambda = 5$  TeV. In addition, we have used mass window as  $M_{e_8} - 40 \text{ GeV} < M_{je^-} < M_{e_8} + 40 \text{ GeV}$  for signal with  $\Lambda = M_{e_8}$  and for background. Since, it is seen from Figure 1, signal decay width values are approximately 20 GeV at the LHeC-2 kinematic limit (2.049 TeV) for the  $\Lambda = M_{e_8}$ . By using this cut sets

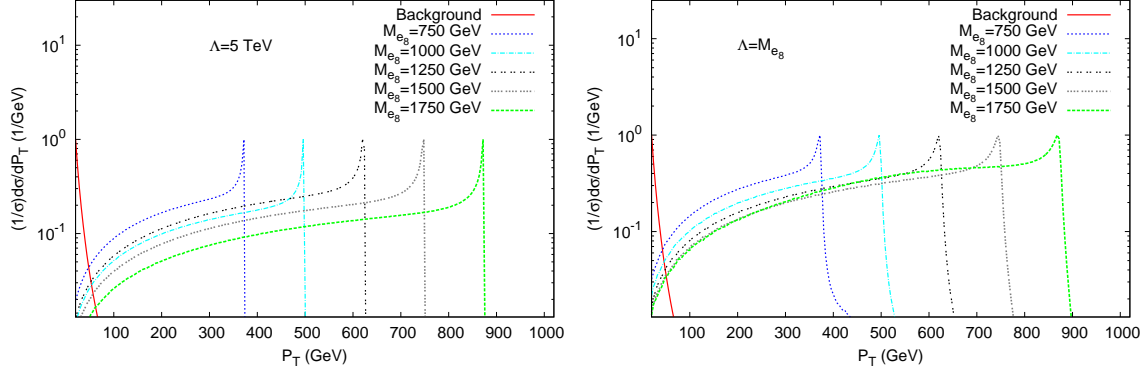


Figure 12. Left: Normalized transverse momentum ( $P_T$ ) distributions of the final state jets for signal with  $\Lambda = 5$  TeV and for background at the LHeC-2. Right: Normalized transverse momentum ( $P_T$ ) distributions of the final state jets for signal with  $\Lambda = M_{e_8}$  TeV and for background at the LHeC-2.

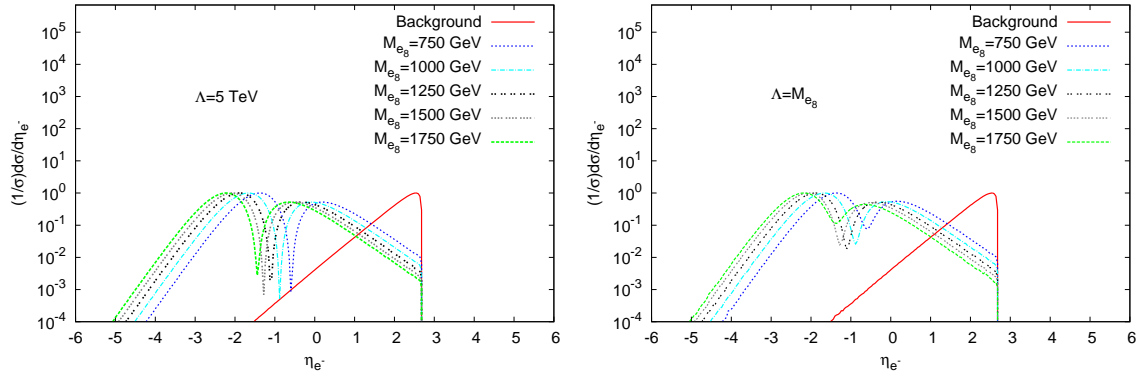


Figure 13. Left: Normalized pseudo-rapidity distributions of final state electrons for signal with  $\Lambda = 5$  TeV and background at the LHeC-2. Right: Normalized pseudo-rapidity distributions of final state electrons for signal with  $\Lambda = M_{e_8}$  and background at the LHeC-2.

and integrated luminosity values of the LHeC-2,  $L_{int} = 1000 \text{ fb}^{-1}$ , we have calculated event numbers of some mass values of  $e_8$  and the background. We present these event numbers in Table 4.

For statistical significance, we have used the Equation 5 and we have presented the statistical significances of spin-3/2 color octet electron signal with  $\Lambda = 10$  TeV,  $\Lambda = 5$  TeV and  $\Lambda = M_{e_8}$  as a function of spin-3/2 color octet electron masses in Figure 16, 17 and 18. Figure 16, 17 and 18 are obtained for LHeC-2 with  $\sqrt{s} = 2.049$  TeV and  $L_{int} = 1000 \text{ fb}^{-1}$ .

As one can see from Figure 16, the upper mass limit for discovery ( $5\sigma$ ) of spin-3/2 color

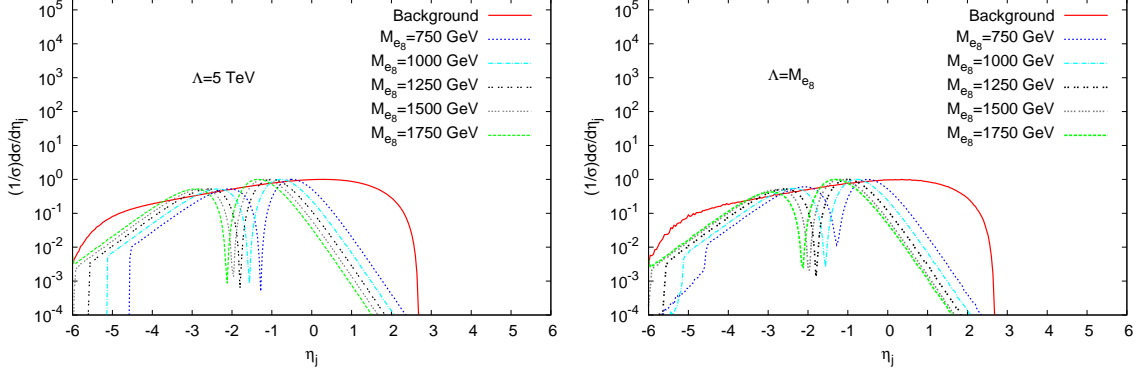


Figure 14. Left: Normalized pseudo-rapidity distributions of final state jets for signal with  $\Lambda = 5$  TeV and background at the LHeC-2. Right: Normalized pseudo-rapidity distributions of final state jets for signal with  $\Lambda = M_{e_8}$  TeV and background at the LHeC-2.

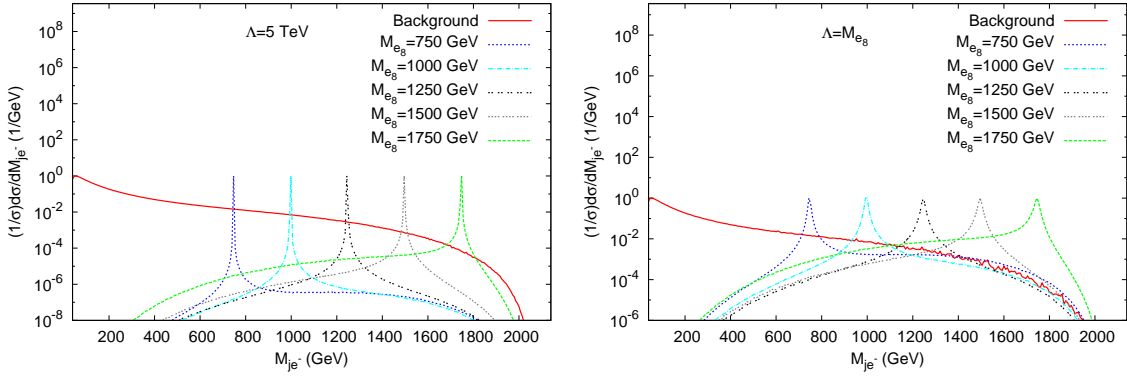


Figure 15. Left: Normalized invariant mass distributions for signal with  $\Lambda = 5$  TeV and background at the LHeC-2. Right: Normalized invariant mass distributions for signal with  $\Lambda = M_{e_8}$  and background at the LHeC-2.

octet electron ( $e_8$ ) is 1.36 TeV at the LHeC-2 with  $\sqrt{s} = 2.049$  TeV. The upper observation ( $3\sigma$ ) mass limit of  $e_8$  is 1.47 TeV and the upper exclusion limit of  $e_8$  is 1.55 TeV. These upper mass values are obtained for  $L_{int} = 1000 \text{ fb}^{-1}$  integrated luminosity and  $\Lambda = 10$  TeV.

It can be seen from Figure 17, the upper mass limit for discovery ( $5\sigma$ ) of spin-3/2 color octet electron ( $e_8$ ) is 1.77 TeV at the LHeC-2 with  $\sqrt{s} = 2.049$  TeV. The upper observation ( $3\sigma$ ) mass limit of  $e_8$  is 1.82 TeV and the upper exclusion limit of  $e_8$  is 1.85 TeV. These upper mass values are obtained for  $L_{int} = 1000 \text{ fb}^{-1}$  integrated luminosity and  $\Lambda = 5$  TeV.

It is seen from Figure 18, the upper mass limit for discovery ( $5\sigma$ ) of spin-3/2 color octet

| $M_{e_8}$ , GeV | $\Lambda = 10$ TeV |                    | $\Lambda = 5$ TeV  |                    | $\Lambda = M_{e_8}$ |                    |
|-----------------|--------------------|--------------------|--------------------|--------------------|---------------------|--------------------|
|                 | $N_s$              | $N_b$              | $N_s$              | $N_b$              | $N_s$               | $N_b$              |
| 500             | $8.3 \times 10^3$  | $7.74 \times 10^4$ | $1.33 \times 10^5$ | $7.75 \times 10^4$ | $1.60 \times 10^9$  | $3.11 \times 10^5$ |
| 750             | $4.61 \times 10^3$ | $3.96 \times 10^4$ | $7.38 \times 10^4$ | $3.96 \times 10^4$ | $1.82 \times 10^8$  | $1.57 \times 10^5$ |
| 1000            | $2.08 \times 10^3$ | $1.20 \times 10^4$ | $3.34 \times 10^4$ | $1.99 \times 10^4$ | $2.66 \times 10^7$  | $7.99 \times 10^4$ |
| 1250            | $6.70 \times 10^2$ | $8.05 \times 10^3$ | $1.07 \times 10^4$ | $8.05 \times 10^3$ | $3.53 \times 10^6$  | $3.18 \times 10^4$ |
| 1500            | $1.19 \times 10^2$ | $2.07 \times 10^3$ | $1.89 \times 10^3$ | $2.07 \times 10^3$ | $3.04 \times 10^5$  | $8.33 \times 10^3$ |
| 1750            | 6                  | $1.99 \times 10^2$ | $9.50 \times 10^1$ | $1.99 \times 10^2$ | $8.40 \times 10^3$  | $8.07 \times 10^2$ |
| 2000            | -                  | -                  | -                  | -                  | 1                   | -                  |

Table IV. The number of signal and background event for the LHeC-2 with  $L_{int} = 1000 \text{ fb}^{-1}$ .  $N_s$  and  $N_b$  represent number of signal and background event, respectively.

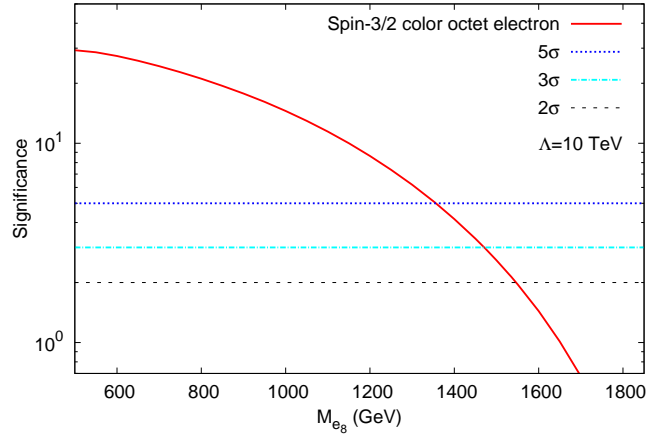


Figure 16. The signal significances as a function of spin-3/2 color octet electron mass at the LHeC-2 with  $\sqrt{s} = 2.049$  TeV. This figure is obtained for  $L_{int} = 1000 \text{ fb}^{-1}$  and  $\Lambda = 10$  TeV.

electron ( $e_8$ ) is 1.95 TeV at the LHeC-2 with  $\sqrt{s} = 2.049$  TeV. The upper observation ( $3\sigma$ ) mass limit of  $e_8$  is 1.97 TeV and the upper exclusion limit of  $e_8$  is 1.98 TeV. These upper mass values are obtained for  $L_{int} = 1000 \text{ fb}^{-1}$  integrated luminosity and  $\Lambda = M_{e_8}$  TeV.

The spin-1/2 color octet electron and the spin-3/2 color octet electron will have the same final state at the LHeC-2 with  $\sqrt{s} = 2.049$  TeV. In order to diverge the spin-3/2 and the spin-1/2 color octet electron signals we plot normalized differential cross section as a function of  $\cos\theta$  in Figure 19 and Figure 20. The spin-1/2 color octet electron is produced mostly



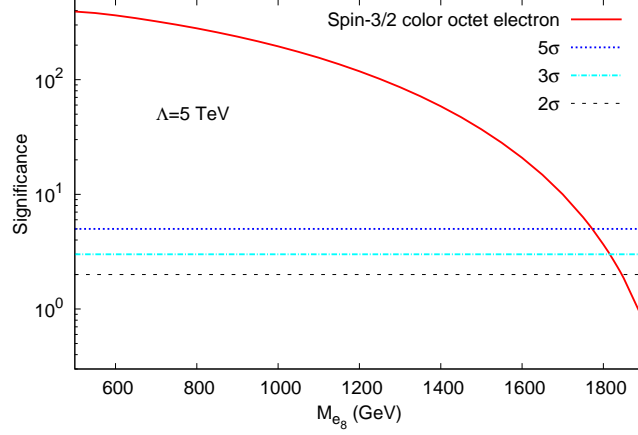


Figure 17. The signal significances as a function of spin-3/2 color octet electron mass at the LHeC-2 with  $\sqrt{s} = 2.049$  TeV. This figure is obtained for  $L_{int} = 1000 \text{ fb}^{-1}$  and  $\Lambda = 5$  TeV.

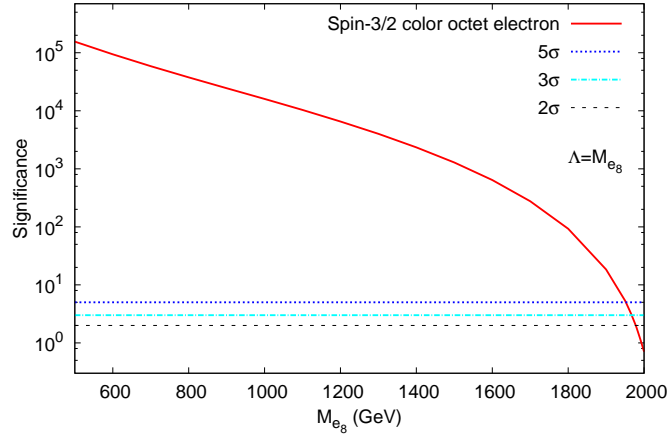


Figure 18. The signal significances as a function of spin-3/2 color octet electron mass at the LHeC-2 with  $\sqrt{s} = 2.049$  TeV. This figure is obtained for  $L_{int} = 1000 \text{ fb}^{-1}$  and  $\Lambda = M_{e_8}$  TeV.

in backward direction and it has its minimum cross section values in forward direction. Whereas, spin-3/2 color octet electron is produced mostly in both directions (forward and backward) and its minimum cross section values are between in -0.4 to -0.3. Therefore, the spin-3/2 color octet electron shows different angular shape from the spin-1/2 color octet electron.

In order to estimate compositeness scale for spin-3/2 color octet electron at the LHeC-2 with  $\sqrt{s} = 2.049$  and  $L_{int} = 1000 \text{ fb}^{-1}$ , we have plot the compositeness scale as a function of spin-3/2 color octet electron mass in Figure 21. We present reachable values of the

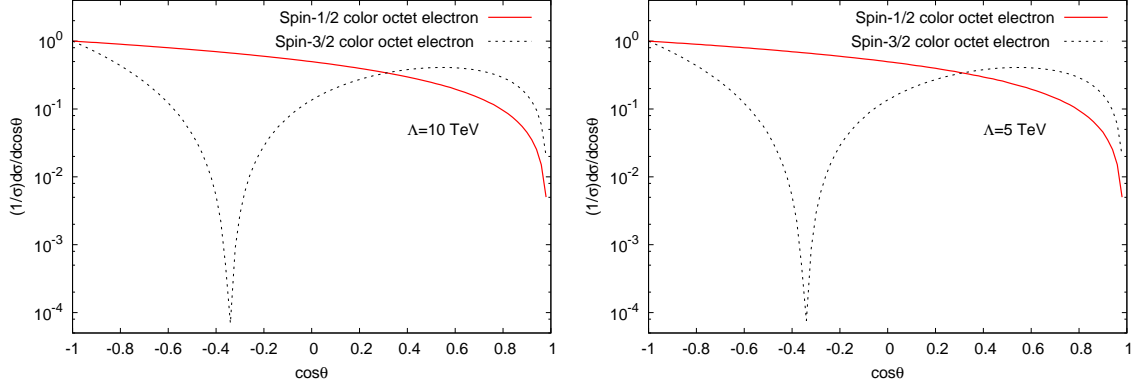


Figure 19. Left: The differential cross section as a function the scattering angle for the spin-3/2 color octet electron ( $\Lambda = 10$  TeV), and the spin-1/2 color octet electron ( $\Lambda = 10$  TeV) at the LHeC-2 with  $\sqrt{s} = 2.049$  TeV. Right: The differential cross section as a function the scattering angle for the spin-3/2 color octet electron ( $\Lambda = 5$  TeV), and the spin-1/2 color octet electron ( $\Lambda = 5$  TeV) at the LHeC-2 with  $\sqrt{s} = 2.049$  TeV. In the both panels, spin-1/2 and spin-3/2 color octet electron mass values are taken as 1 TeV.

compositeness scale for some color octet electron mass values in Table 5. It can be seen from Table 5, the spin-3/2 color octet electron with  $M_{e_8} = 1$  TeV can be discovered up to 13.1 TeV compositeness scale value at the LHeC-2 with  $\sqrt{s} = 2.049$  TeV and  $L_{int} = 1000 \text{ fb}^{-1}$ .

#### IV. CONCLUSION

We have performed a search for resonant production of spin-3/2 color octet electron at the LHeC. We show that if the compositeness scale ( $\Lambda$ ) equals to 5 TeV, LHeC-1 with  $\sqrt{s} = 1.296$  and  $L_{int} = 10 \text{ fb}^{-1}$  will give the opportunity to discovery chance up to  $M_{e_8} = 660$  GeV and observation chance up to  $M_{e_8} = 777$  GeV for spin-3/2 color octet electron. In addition, LHeC-1 give the opportunity for exclusion of spin-3/2 color octet electron up to 849 GeV. When we consider  $\Lambda = M_{e_8}$  and  $L_{int} = 10 \text{ fb}^{-1}$  case, upper mass values of the spin-3/2 color octet electron are 1.19 TeV for discovery ( $5\sigma$ ), 1.21 TeV for observation ( $3\sigma$ ) and 1.22 TeV for exclusion ( $2\sigma$ ).

LHeC-2 with  $\sqrt{s} = 2.049$  TeV and  $L_{int} = 1000 \text{ fb}^{-1}$  will give the opportunity to discovery ( $5\sigma$ ) up to  $M_{e_8} = 1.36$  TeV, observation ( $3\sigma$ ) up to  $M_{e_8} = 1.47$  TeV and exclusion ( $2\sigma$ ) up to  $M_{e_8} = 1.55$  TeV for spin-3/2 color octet electron with  $\Lambda = 10$  TeV. At the LHeC-2 with

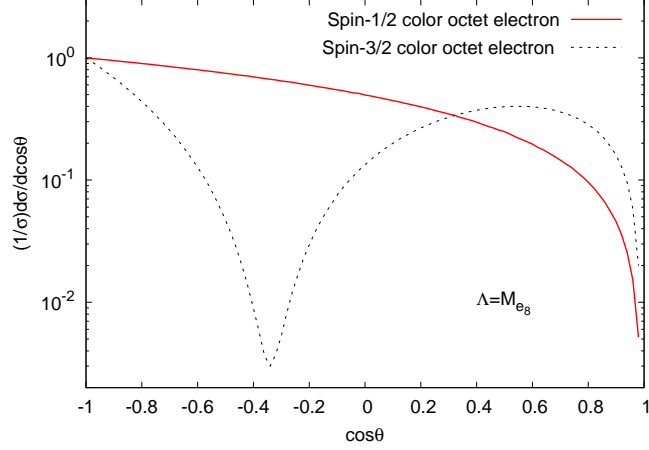


Figure 20. The differential cross section as a function the scattering angle for the spin-3/2 color octet electron ( $\Lambda = M_{e_8}$ ), and the spin-1/2 color octet electron ( $\Lambda = M_{e_8}$ ) at the LHeC-2 with  $\sqrt{s} = 2.049$  TeV. The spin-1/2 and the spin-3/2 color octet electron mass values are taken as 1 TeV in our calculations.

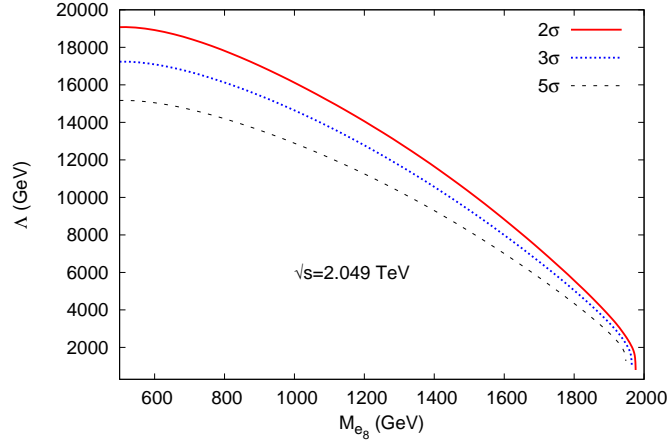


Figure 21. Reachable values of the compositeness scale as a function of spin-3/2 color octet electron mass for the LHeC-2 with  $\sqrt{s} = 2.049$  TeV and  $L_{int} = 1000 \text{ fb}^{-1}$ .

$\sqrt{s} = 2.049$  TeV and  $L_{int} = 1000 \text{ fb}^{-1}$ , these upper mass values are 1.77 TeV for discovery ( $5\sigma$ ), 1.82 TeV for observation ( $3\sigma$ ) and 1.85 TeV for exclusion ( $2\sigma$ ) of spin-3/2 color octet electron with  $\Lambda = 5$  TeV. For spin-3/2 color octet electron with  $\Lambda = M_{e_8}$ , we find out that the discovery limit ( $5\sigma$ ) is 1.95 TeV, the observation limit is 1.97 TeV and the exclusion limit is 1.98 TeV at the LHeC-2 with  $\sqrt{s} = 2.049$  TeV and  $L_{int} = 1000 \text{ fb}^{-1}$ .

We also show that LHeC-1 with  $\sqrt{s} = 1.296$  TeV and  $L_{int} = 10 \text{ fb}^{-1}$  will give the

| $M_{e_8}$ , GeV | $\Lambda$ , TeV |           |           |
|-----------------|-----------------|-----------|-----------|
|                 | $5\sigma$       | $3\sigma$ | $2\sigma$ |
| 500             | 15.6            | 17.7      | 19.6      |
| 600             | 15.4            | 17.5      | 19.3      |
| 700             | 14.9            | 17.0      | 18.8      |
| 800             | 14.4            | 16.4      | 18.1      |
| 900             | 13.8            | 15.7      | 17.3      |
| 1000            | 13.1            | 14.9      | 16.5      |
| 1100            | 12.3            | 14.0      | 14.9      |
| 1200            | 11.5            | 13.1      | 14.5      |
| 1300            | 10.6            | 12.0      | 13.3      |
| 1400            | 9.6             | 10.9      | 12.0      |
| 1500            | 8.5             | 9.6       | 10.7      |
| 1600            | 7.3             | 8.3       | 9.2       |
| 1700            | 6.0             | 6.9       | 7.6       |
| 1800            | 4.6             | 5.3       | 5.9       |
| 1900            | 3.0             | 3.5       | 3.9       |

Table V. Reachable values of the compositeness scale for some spin-3/2 electrons mass values at the LHeC-2 with  $\sqrt{s} = 2.049$  TeV and  $L_{int} = 1000 \text{ fb}^{-1}$ .

opportunity for discovery ( $5\sigma$ ) of  $e_8$  with  $M_{e_8} = 500$  GeV up to  $\Lambda = 5.68$  TeV. We will observe ( $3\sigma$ )  $e_8$  with  $M_{e_8} = 500$  GeV up to  $\Lambda = 6.47$  TeV and exclude ( $2\sigma$ )  $e_8$  with  $M_{e_8} = 500$  GeV up to  $\Lambda = 7.17$  TeV at the LHeC-1 with  $\sqrt{s} = 1.296$  TeV and  $L_{int} = 10 \text{ fb}^{-1}$  (see Table 3). LHeC-2 with  $\sqrt{s} = 2.049$  TeV and  $L_{int} = 1000 \text{ fb}^{-1}$  will give opportunity for discovery of  $e_8$  with  $M_{e_8} = 500$  GeV up to  $\Lambda = 15.6$  TeV. We will observe  $e_8$  with  $M_{e_8} = 500$  GeV up to  $\Lambda = 17.8$  TeV and exclude  $e_8$  with  $M_{e_8} = 500$  GeV up to  $\Lambda = 19.6$  TeV at the LHeC-2 with  $\sqrt{s} = 2.049$  and  $L_{int} = 1000 \text{ fb}^{-1}$ . LHeC-2 with  $\sqrt{s} = 2.049$  and  $L_{int} = 1000 \text{ fb}^{-1}$  will give opportunity for discovery ( $5\sigma$ ) of  $e_8$  with  $M_{e_8} = 1$  TeV up to  $\Lambda = 13.1$  TeV. We will observe  $e_8$  with  $M_{e_8} = 1$  TeV up to  $\Lambda = 14.9$  TeV and exclude  $e_8$  with  $M_{e_8} = 1$  TeV up to  $\Lambda = 16.5$  TeV at the LHeC-2 (see Table V).

## ACKNOWLEDGMENTS

I would like to thank Saleh Sultansoy and Gökhan Ünel for their useful discussions and helpful comments. This work is supported by TUBITAK BIDEB-2219 grant.

---

- [1] G. Aad *et al.* (ATLAS Collaboration), Phys. Lett. B **716**, 1 (2012); arXiv:1207.7214 [hep-ex].
- [2] S. Chatrchyan *et al.* (CMS Collaboration), Phys. Lett. B **716**, 30 (2012); arXiv:1207.7235 [hep-ex].
- [3] I. A. D’Souza and C. S. Kalman, PREONS: Models of Leptons, Quarks and Gauge Bosons as Composite Objects, World Scientific Publishing Co., 1992.
- [4] H. Harari, Phys. Lett. B **86**, 83 (1979).
- [5] H. Fritzsch, G. Mandelbaum, Phys. Lett. B **102**, 319 (1981).
- [6] O. W. Greenberg, J. Sucher, Phys. Lett. B **99**, 339 (1981).
- [7] R. Barbieri, R. N. Mohapatra, A. Maseiro, Phys. Lett. B **105**, 369 (1981).
- [8] U. Baur, K. H. Streng, Phys. Lett. B **162**, 387 (1985).
- [9] A. Celikel, M. Kantar, S. Sultansoy, Phys. Lett. B **443**, 359 (1998).
- [10] J. Leite Lopes, J. A. Martins Simoes and D. Spehler, Phys. Lett. B **94**, 367 (1980); Phys. Rev. D **23**, 797 (1981); D **25**, 1854 (1982).
- [11] Y. Tosa and R. E. Marshak, Phys. Rev. D **32**, 774 (1985).
- [12] P. van Nieuwenhuizen, Phys. Rep. **68**, 774 (1985).
- [13] T. G. Rizzo, Phys. Rev. D **33**, 1852 (1986).
- [14] T. G. Rizzo, Phys. Rev. D **34**, 133 (1986).
- [15] K. H. Streng, Z. Phys. C **33**, 247 (1986).
- [16] J. L. Hewett and T. G. Rizzo, Phys. Rev. D **56**, 5709 (1997); [hep-ph/9703337].
- [17] A. Celikel and M. Kantar, Turk. J. Phys. **22**, 401 (1998).
- [18] M. Sahin, S. Sultansoy and S. Turkoz, Phys. Lett. B **689**, 172 (2010); [arXiv:1001.4505 [hep-ph]].
- [19] A. N. Akay, H. Karadeniz, M. Sahin and S. Sultansoy, Europhys. Lett. **95**, 31001 (2011); [arXiv:1012.0189 [hep-ph]].
- [20] Tanumoy Mandal and Subhadip Mitra, Phys. Rev. D **87**, 095008 (2013); [arXiv:1211.6394v1]

- [hep-ph]].
- [21] The LHeC web page, <http://www.lhec.org.uk>.
  - [22] J. L. Abelleira Fernandez et al. [LHeC Study Group Collaboration], J. Phys. G **39**, 075001 (2012); [arXiv:1206.2913 [physics.acc-ph]].
  - [23] CERN-ECFA-NuPECC Workshop on the LHeC, Chavannes, Switzerland, June 2012, see <http://cern.ch/lhec>.
  - [24] J. L. Abelleira Fernandez et al. [LHeC Study Group Collaboration], [arXiv:1211.4831 [hep-ex]].
  - [25] A. N. Akay, H. Karadeniz, and S. Sultansoy, Int. J. Mod. Phys. A **25**, 4589 (2010).
  - [26] W. Rarita and J. Schwinger, Phys. Rev. D **60**, 61 (1941).
  - [27] A. Pukhov et al., hep-ph/9908288.
  - [28] Alexander Belyaev, Neil D. Christensen, Alexander Pukhov, [arXiv:1207.6082 [hep-ph]].
  - [29] J. Pumplin et al., J. High Energy Phys. **07**, 012 (2002); D. Stump et al., J. High Energy Phys. **10**, 046 (2003).
  - [30] G. L. Bayatian et al. (CMS Collaboration), J. Phys. G **34**, 995 (2007).
  - [31] J. Beringer et al. (Particle Data Group), Phys. Rev. D **86**, 010001 (2012).